

Article

# Traversability Analysis and Path Planning for Autonomous Wheeled Vehicles on Rigid Terrains

Nan Wang<sup>1</sup>, Xiang Li<sup>1</sup>, Zhe Suo<sup>1</sup>, Jiuchen Fan<sup>2</sup>, Jixin Wang<sup>1,\*</sup> and Dongxuan Xie<sup>3,4,5,\*</sup>

<sup>1</sup> Key Laboratory of CNC Equipment Reliability, Ministry of Education, School of Mechanical and Aerospace Engineering, Jilin University, Changchun 130022, China; nwang22@mails.jlu.edu.cn (N.W.); lixiang\_sub@163.com (X.L.); suozhe23@mails.jlu.edu.cn (Z.S.)

<sup>2</sup> College of Mechanical Engineering, Beihua University, Jilin 132021, China; fanjiuchen1973@163.com

<sup>3</sup> School of Computer Science and Engineering, Changchun University of Technology, Changchun 130012, China

<sup>4</sup> Northeast Industries Group Co., Ltd., Changchun 130103, China

<sup>5</sup> School of Vehicle and Mobility, Tsinghua University, Beijing 100084, China

\* Correspondence: jxwang@jlu.edu.cn (J.W.); xiedongxuan@ccut.edu.cn (D.X.)

**Abstract:** Autonomous vehicles play a crucial role in three-dimensional transportation systems and have been extensively investigated and implemented in mining and other fields. However, the diverse and intricate terrain characteristics present challenges to vehicle traversability, including complex geometric features such as slope, harsh physical parameters such as friction and roughness, and irregular obstacles. The current research on traversability analysis primarily emphasizes the processing of perceptual information, with limited consideration for vehicle performance and state parameters, thereby restricting their applicability in path planning. A framework of traversability analysis and path planning methods for autonomous wheeled vehicles on rigid terrains is proposed in this paper for better traversability costs and less redundancy in path planning. The traversability boundary conditions are established first based on terrain and vehicle characteristics using theoretical methods to determine the traversable areas. Then, the traversability cost map for the traversable areas is obtained through simulation and segmented linear regression analysis. Afterward, the TV-Hybrid A\* algorithm is proposed by redefining the path cost functions of the Hybrid A\* algorithm through the simulation data and neural network method to generate a more cost-effective path. Finally, the path generated by the TV-Hybrid A\* algorithm is validated and compared with that of the A\* and Hybrid A\* algorithms in simulations, demonstrating a slightly better traversability cost for the former.

**Keywords:** unmanned ground vehicle (UGV); three-dimensional transportation systems; unstructured environment; traversability analysis; path planning



**Citation:** Wang, N.; Li, X.; Suo, Z.; Fan, J.; Wang, J.; Xie, D. Traversability Analysis and Path Planning for Autonomous Wheeled Vehicles on Rigid Terrains. *Drones* **2024**, *8*, 419. <https://doi.org/10.3390/drones8090419>

Academic Editor: Oleg Yakimenko

Received: 30 July 2024

Revised: 21 August 2024

Accepted: 22 August 2024

Published: 23 August 2024



**Copyright:** © 2024 by the authors. Licensee MDPI, Basel, Switzerland. This article is an open access article distributed under the terms and conditions of the Creative Commons Attribution (CC BY) license (<https://creativecommons.org/licenses/by/4.0/>).

## 1. Introduction

Three-dimensional transportation enhances traffic efficiency and safety by utilizing advanced technical means and facilities. Autonomous vehicles are integral to this system in various fields, including mining, rescue, construction, and military operations [1–3]. The roads of these applications typically are rigid terrains. Rigid terrains encompass compacted soil, asphalt, or concrete surfaces, which typically exhibit negligible deformation under loading, as demonstrated in Figure 1. Surface coverings such as snow, dust, and grass, along with the roughness of rigid terrains, not only reduce contact friction but can contribute to amplified driving vibrations. The geometric features (e.g., slope) and irregular terrain obstacles (e.g., ditches, steps, vegetation) of rigid terrains also present a formidable challenge to vehicle traversability.

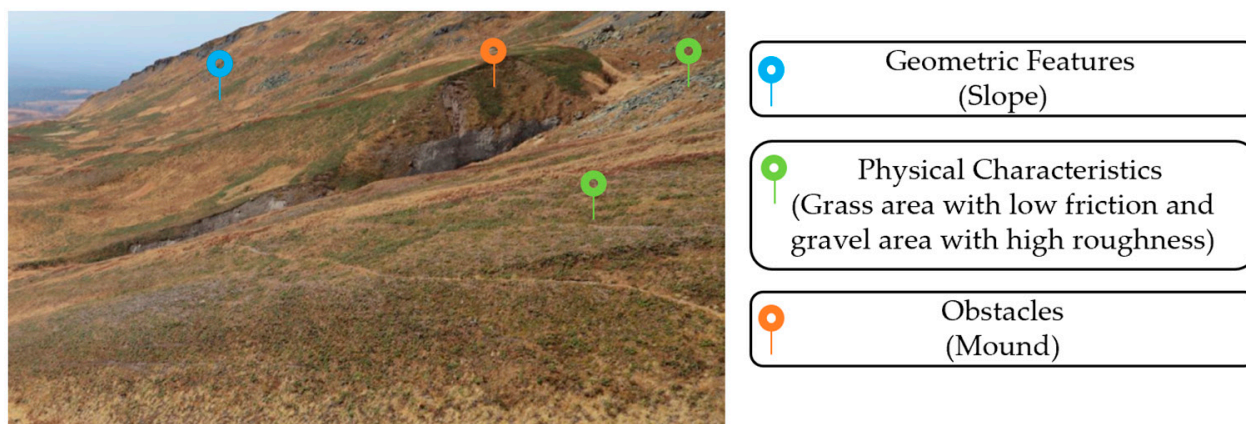


**Figure 1.** An example of rigid terrain composed of compacted soil.

Traversability analysis typically evaluates a vehicle's ability to navigate specific areas based on environmental and vehicle information [4]. Estimating traversability is crucial for autonomous path planning in unstructured environments. Inaccurate or inefficient assessment of traversability can lead to the generation of subpar paths, resulting in excessive energy and time consumption as well as unnecessary risks to equipment and the environment [4,5].

Although vehicles are capable of traversing certain areas, they may incur additional costs such as safety expenses, energy consumption, time expenditure, speed reduction, and wear and tear on parts or goods. Therefore, it is essential to assess the cost of terrain traversability. The results of a traversability cost analysis can provide valuable information for path planners to select and optimize the path.

This paper integrates environmental data such as terrain geometric features, physical parameters, static obstacle information, and wheeled vehicle characteristics using theoretical methods to establish traversability boundary conditions and generate a traversability boundary map for specific areas. The traversability boundary map is utilized to delineate the traversable boundary while excluding impassable areas for subsequent construction of the cost map and path planning to enhance efficiency. Then, simulation and segmented linear regression are combined to conduct a comprehensive analysis of traversability costs and generate a multi-layer traversability cost map based on the established cost functions. This paper not only takes into account the vehicle dimensions and performance parameters but also considers the speed, load, tire pressure, and other vehicle state parameters. Subsequently, the TV-Hybrid A\* algorithm is proposed for path planning by redefining the cost function of the Hybrid A\* algorithm based on simulation test data and a neural network method to account for the impact of rigid terrains on vehicle path costs.

The contributions of this paper include the following:

- An optimized framework for path planning on rigid terrains is introduced aimed at minimizing redundant efforts and enhancing overall operational efficiency, as illustrated in Figure 2.
- Methods of assessing the traversability boundaries and costs on rigid terrains are proposed by the theory-based and segmented linear regression approach taking into consideration terrain and vehicle characteristics.
- The TV-Hybrid A\* algorithm, a path planning algorithm for rigid terrains, is proposed based on the Hybrid A\* algorithm with a three-layer neural network model to improve cost functions.

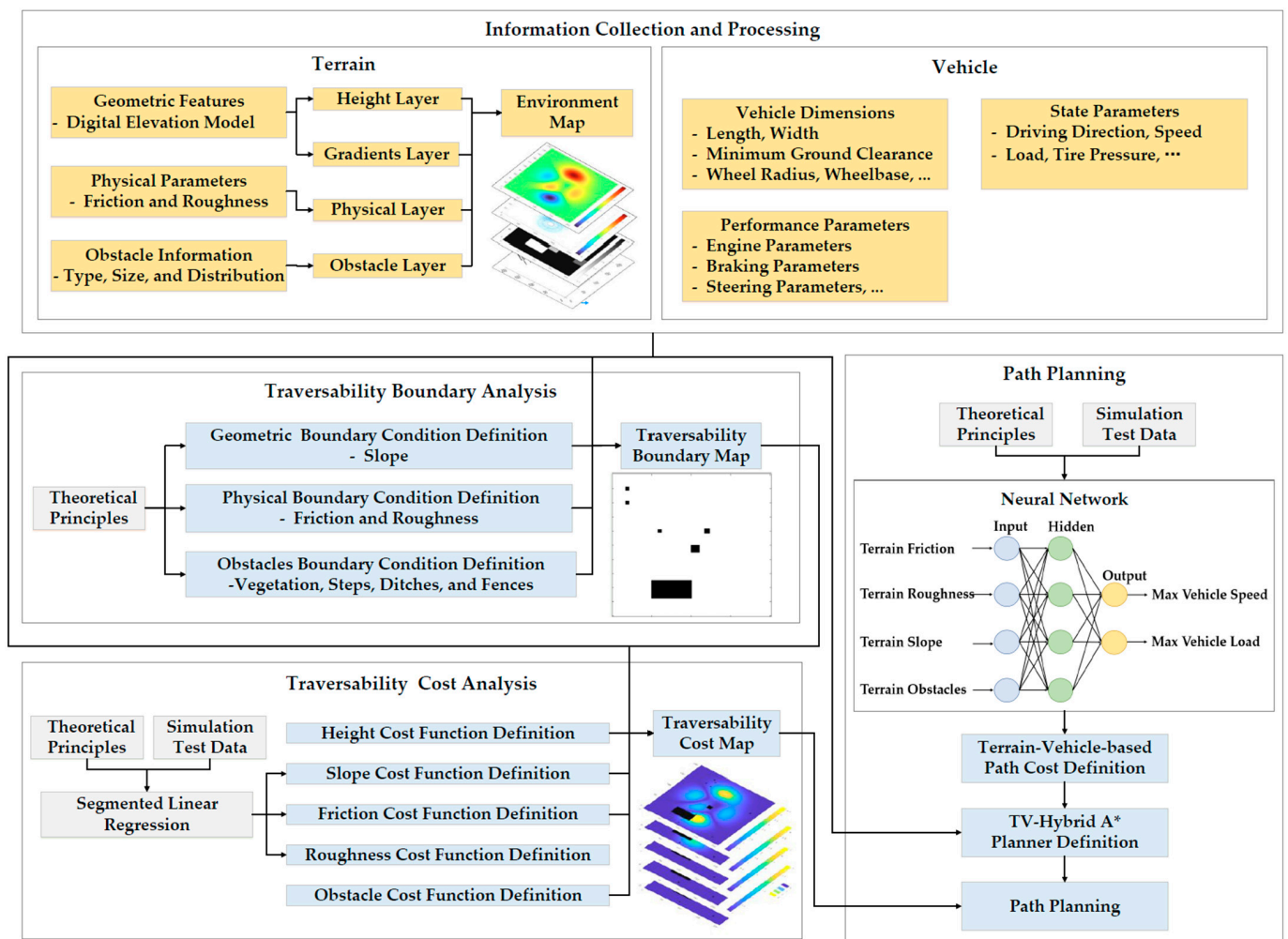


**Figure 2.** The proposed framework of traversability analysis and path planning methods for autonomous wheeled vehicles on rigid terrains.

## 2. Related Work

### 2.1. Traversability Analysis

Currently, the focus of traversability analysis lies in environmental perception, particularly in the methods for collecting and processing perceived environmental data [6–8]. The means of traversability analysis typically include experimental, image processing-based, and behavior-based approaches [5]. Early traversability analysis was usually conducted through experiments. For example, the cone index method was proposed by the Waterways Experiment Station (WES) of the U.S. military to determine the traversability of a particular vehicle in a certain soil [9]. The experimental methods are expensive, time-consuming, and also constrained by environmental limitations and challenges in replication [5]. As a result, simulation tests have become widely adopted. Image processing-based methods typically rely on geometric and semantic information to make assessments, but they fail to consider the vehicle performance parameters and the terrain physical attributes [10]. Behavior-based methods, which are the new trend in this field, assess the traversability by experts' driving trajectories with learning-based methods [11–13]. These methods are tailored to specific vehicles and are not directly applicable to different vehicles or even the same vehicle under varying operating conditions [14]. Hence, it is strongly advised to utilize traversability analysis means that integrate theoretical principles, simulation techniques, and machine learning algorithms [5,7].

The outputs of a traversability analysis can be categorized into classification-based and regression-based results. Classification-based results are generally discrete classes of

terrain type, including binary classification and multi-classification [15]. Classification-based methods often provide restricted traversability analysis for specific categories, and their results are challenging to directly integrate into the path planner [7]. The outcomes derived from regression-based methods are depicted as traversability maps or functions, which can be readily fed into the path planner [16].

Traversability analysis is closely tied to the vehicle characteristics. Reference [17] first generates a geometric representation of the world, then assesses traversability by comparing the geometric features such as the height, width, and slope of the traversable areas with the vehicle dimensions. Additionally, traversability is also impacted by the performance and state parameters of vehicles. For example, the vehicle's capability to traverse slopes varies depending on the vehicle's driving direction, speed, and load. Indeed, current research has given scant attention to these crucial aspects, significantly limiting their practical applicability within the realm of path planning. This paper aims to address this gap by first defining the traversability boundary condition from a vehicle performance perspective based on mechanics theory and then determining the traversability cost through a segmented linear regression method using the simulation results of vehicle traversability under different terrain parameters.

## 2.2. Path Planning

In recent years, the predominant path planning strategies for rigid terrains encompass graph-search-based, sampling-based, and artificial potential field (APF) approaches [5,18]. Among these, graph-search-based methods can effectively integrate the results of traversability cost analysis [7]. Graph-search-based methods discretize the configuration space as a graph and then search for a minimum-cost path within it [19,20]. The A\* and Dijkstra are the most common algorithms [21].

A\* search can be seen as an improvement of Dijkstra's search [22,23]. The A\* algorithm was proposed by Hart in the 1960s, combining the advantages of the mathematical search method and the heuristic search method. By using a heuristic function to guide the search direction, it can reduce the search amount, improve the efficiency of the algorithm, and ensure the optimization of the results [24].

The Hybrid A\* algorithm represents a significant enhancement of the A\* algorithm [22], which is limited to considering positions in two dimensions ( $x, y$ ), while the Hybrid A\* algorithm incorporates vehicle kinematic constraints and introduces an additional dimension  $\theta$  (the direction of the vehicle) to optimize node expansion for better alignment with the motion characteristics of the vehicle. The path points generated by the A\* algorithm typically fall within the center of the grid, whereas those produced by the Hybrid A\* algorithm have the potential to appear anywhere within the grid, resulting in a more adaptable and seamless path. The heuristic function of the A\* algorithm typically relies on straightforward distance estimation, such as the Euclidean or Manhattan distance. In contrast, the Hybrid A\* algorithm takes into account real-world factors and introduces penalties for variables such as the vehicle angle, gear changes, and forward/backward motion adjustments to ensure that the planned trajectory aligns more closely with actual motion scenes. However, the path cost function for both Hybrid A\* and A\* does not take into account the impact of terrain physical parameters and obstacles on vehicle traversability. Therefore, the path cost function of Hybrid A\* is improved in this paper with the simulation data and a three-layer neural network model to generate a more cost-effective path.

## 3. Methods

### 3.1. Overview

The overall framework of traversability analysis and path planning methods on rigid terrains proposed in this paper is illustrated in Figure 2. The environmental information collected in this study is processed to generate a multi-layer map, which includes a 2.5D height layer, a gradient layer, a terrain physical characteristics layer, and a static obstacle layer. Then, theoretical principles are applied based on wheeled vehicle characteristics to

define the boundary conditions for the terrain geometric features, physical parameters, and static obstacles. The wheeled vehicle characteristics considered in this paper encompass structural dimensions (e.g., vehicle length, vehicle width, minimum ground clearance, wheel radius, wheelbase), performance parameters (e.g., maximum engine torque, maximum engine speed, maximum engine power, maximum braking torque, minimum turning radius, maximum steering angle), and state parameters (e.g., driving direction, speed, load, tire pressure). Based on the established boundary conditions, a traversability boundary map is generated from the initial environment map while eliminating impassable areas.

A multi-layer cost map for the traversable areas is generated by conducting a terrain traversability cost analysis, taking into account the terrain height, slope, friction, roughness, and obstacles. The estimation of terrain slope, friction, and roughness costs is established using simulation test data and the segmented linear regression method. The traversability cost of terrain obstacles is empirically determined based on their impact on the wheeled vehicle driving speed.

Path planning is conducted based on the traversability boundary map and cost map. This paper proposes the TV-Hybrid A\* planner by introducing the consideration of terrain characteristics into the Hybrid A\* planner to comprehensively account for various parameters' influence on the path cost function and to thus obtain a more optimized path. The weights of different terrain parameters' influence on the wheeled vehicle path cost are determined by a three-layer neural network model.

### 3.2. Traversability Boundary Analysis

The acquired DEM data are processed to generate a 2.5D height map and gradient map. The terrain physical map with friction and roughness distribution, as well as the static obstacle map, are overlaid as the initial environment map. Subsequently, based on theoretical principles, the traversability boundary conditions for wheeled vehicles in relation to different terrain geometric features, physical parameters, and static obstacles are analyzed sequentially. Finally, impassable areas are removed from the initial environmental representation according to the established boundary conditions to obtain a traversability boundary map to avoid redundancy in cost analysis and path planning.

#### 3.2.1. Terrain Geometric Boundary Condition Definition

The geometric feature that significantly affects vehicle traversability is slope, which is associated with driving direction. In this paper, the limit value of the slope  $S_L$  is defined as:

$$S_L = \min\{slope_{long\_uphill}, slope_{long\_downhill}, slope_{side}\} \quad (1)$$

where  $slope_{long\_uphill}$ ,  $slope_{long\_downhill}$ , and  $slope_{side}$  are the maximum longitudinal uphill slope, the maximum longitudinal downhill slope, and the maximum side slope, respectively, that the wheeled vehicle is capable of traversing.

The maximum longitudinal uphill slope  $slope_{long\_uphill}$  is primarily determined by wheeled vehicle dynamics and static non-pitch performance requirements:

$$slope_{long\_uphill} = \min\{slope_{lu\_d}, slope_{lu\_s}\} \quad (2)$$

where  $slope_{lu\_d}$  and  $slope_{lu\_s}$  are the maximum longitudinal uphill driving slopes required by dynamics and static non-pitch performance, respectively.  $slope_{lu\_s}$  can be calculated by reference [25].  $slope_{lu\_d}$  can be calculated according to the vehicle dynamics equation, disregarding wind resistance and acceleration resistance:

$$slope_{lu\_s} = \tan^{-1} \frac{l_2}{h} \quad (3)$$

$$\begin{cases} F_t = F_f + F_i \\ F_t = \frac{T_{iq} \cdot i}{r} \\ F_f = \varphi \cdot G \cdot \cos(\text{slope}_{l_{u,d}}) \\ F_i = G \cdot \sin(\text{slope}_{l_{u,d}}) \end{cases} \quad (4)$$

where  $l_2$  is the longitudinal distance from the vehicle's center of mass to the center of the vehicle rear axis;  $h$  is the height of the vehicle's center of mass;  $F_t$  is the driving force of the vehicle;  $F_f$  is the friction force of the vehicle;  $F_i$  is the force caused by the slope;  $G$  is the vehicle gravity;  $T_{iq}$  is the torque of the engine or motor;  $i$  is the gear ratio;  $r$  is the driving radius of the wheel, which is influenced by factors such as tire pressure, load, and driving speed; and  $\varphi$  is the terrain friction coefficient.

The maximum longitudinal downhill slope  $\text{slope}_{\text{long\_downhill}}$  is primarily determined by wheeled vehicle dynamics and static non-pitch performance requirements:

$$\text{slope}_{\text{long\_downhill}} = \min\{\text{slope}_{l_{d,d}}, \text{slope}_{l_{d,s}}\} \quad (5)$$

where  $\text{slope}_{l_{d,d}}$  and  $\text{slope}_{l_{d,s}}$  are the maximum longitudinal downhill driving slopes required by dynamics and static non-pitch performance, respectively.  $\text{slope}_{l_{d,s}}$  can be calculated by reference [25].  $\text{slope}_{l_{d,d}}$  can be calculated according to the vehicle dynamics equation, disregarding wind resistance and acceleration resistance:

$$\text{slope}_{l_{d,s}} = \tan^{-1} \frac{l_1}{h} \quad (6)$$

$$\begin{cases} F_i = F_f + F_\mu \\ F_i = G \cdot \sin(\text{slope}_{l_{d,d}}) \\ F_f = \varphi \cdot G \cdot \cos(\text{slope}_{l_{d,d}}) \end{cases} \quad (7)$$

where  $l_1$  is the longitudinal distance from the vehicle's center of mass to the center of the vehicle front axis, and  $F_\mu$  is the braking force.

The maximum side slope  $\text{slope}_{\text{side}}$  is primarily determined by wheeled vehicle dynamics and static non-rollover performance requirements:

$$\text{slope}_{\text{side}} = \min\{\text{slope}_{s,d}, \text{slope}_{s,s}\} \quad (8)$$

where  $\text{slope}_{s,d}$  and  $\text{slope}_{s,s}$  are the maximum side driving slopes required by dynamics and static non-rollover performance, respectively.  $\text{slope}_{s,s}$  can be calculated by reference [25].  $\text{slope}_{s,d}$  can be calculated according to the vehicle dynamics equation, disregarding wind resistance and acceleration resistance:

$$\text{slope}_{s,s} = \min\left\{\tan^{-1} \frac{d_l}{h}, \tan^{-1} \frac{d_r}{h}\right\} \quad (9)$$

$$\begin{cases} F_f = F_s + F_i \\ F_i = G \cdot \sin(\text{slope}_{s,d}) \\ F_f = \varphi \cdot G \cdot \cos(\text{slope}_{s,d}) \end{cases} \quad (10)$$

where  $d_l$  and  $d_r$  are the lateral distances from the vehicle's center of mass to the center of the left and right wheels, respectively, and  $F_s$  is the lateral force that is related to the steering.

### 3.2.2. Terrain Physical Boundary Condition Definition

The primary physical attributes of rigid terrains consist of friction and roughness. In this paper, the limit value of the friction  $\varphi_L$  is defined as:

$$\varphi_L = \min\{\varphi_{L_{acc}}, \varphi_{L_{dec}}\} \quad (11)$$

where  $\varphi_{L_{acc}}$  and  $\varphi_{L_{dec}}$  are the limit values of friction required by a vehicle to drive stably without skidding during acceleration and braking, respectively.  $\varphi_{L_{acc}}$  and  $\varphi_{L_{dec}}$  can be calculated according to the following equations:

$$\varphi_{L_{acc}} = \frac{T_{iq} \cdot i}{N \cdot r} \quad (12)$$

$$\varphi_{L_{dec}} = \frac{m \cdot a_{dec}}{N} \quad (13)$$

where  $m$  is the mass of the vehicle, which is related to the load, and  $a_{dec}$  is the maximum braking deceleration.

The terrain roughness  $R_L$  can be classified into A to H grades according to ISO 8608 [26]. The vehicle's ability to traverse rough roads is influenced by factors such as the vehicle's characteristics (e.g., load, tires, suspension system, chassis height, powertrain), and terrain friction. The thresholds can be determined through experiments or simulation tests, taking into account the transportation, comfort, and wear requirements.

### 3.2.3. Terrain Obstacle Boundary Condition Definition

The boundary conditions of terrain obstacles are analyzed based on the wheeled vehicle characteristics and obstacle information, utilizing both empirical knowledge and theoretical principles. This paper primarily focuses on discrete, densely distributed, and continuous obstacles, such as vegetation, steps, ditches, and fences. Small and single-point obstacles are generally considered in trajectory planning, while large obstacles such as buildings and mountains are treated as impassable areas.

The traversability of vegetation needs to consider both its distribution and height. For discrete vegetation, the wheeled vehicle can pass if the minimum distance between adjacent plants  $BV_{Dis}$  meets Inequality (14). In the case of densely distributed and continuous vegetation, the wheeled vehicle can pass if its minimum ground clearance  $V_{mgc}$  and the height of the plant  $BV_H$  meet Inequality (15). Otherwise, the traversability of vegetation is not recommended for safety reasons.

$$BV_{Dis} \geq V_w + S_w \quad (14)$$

$$BV_H \leq V_{mgc} - S_H \quad (15)$$

where  $V_w$  is the width of the vehicle,  $S_w$  is the safe lateral distance, and  $S_H$  is the safe altitude distance.

The traversability of steps should also take into account their distribution. For a single step, the passable height of the step  $BS_H$  is defined as the minimum value of the maximum heights that the front and rear wheels of the vehicle can cross, as well as the vehicle's minimum ground clearance (see Equation (16)). When dealing with multiple steps, it is also essential to determine whether the minimum interval between adjacent steps  $BS_{Dis}$  allows for the vehicle to pass through after all wheels have landed in a steady state (see Inequality (17)). If not, when the front wheels are ready to pass over one step but the rear wheels have not completely passed over the previous step, it is not recommended for safety and stability reasons.

$$BS_H = \min\{BS_{HF}, BS_{HR}, V_{mgc}\} \quad (16)$$

$$BS_{Dis} > V_{lb} \quad (17)$$

where  $BS_{HF}$  and  $BS_{HR}$  are the maximum heights that the front and rear wheels of the vehicle can cross, which can be calculated by reference [9] (see Equations (18) and (19)).  $V_{lb}$  is the wheelbase of the vehicle.

$$BS_{HF} = r \cdot \frac{1 - \varphi \frac{r}{V_{lb}} + \eta^2 - \eta \cdot \sqrt{1 - 2\varphi \frac{r}{V_{lb}} + \eta^2}}{\left(1 + \varphi \frac{r}{V_{lb}}\right)^2 + \eta^2} \quad (18)$$

$$\left\{ \begin{array}{l} \left\{ \varphi \frac{r}{V_{lb}} + \left[ -\varphi^2 + (1 + \varphi^2) \frac{l}{V_{lb}} \right] \cos \beta + \left[ \varphi - (1 + \varphi^2) \frac{h}{V_{lb}} \right] \sin \beta \right\} \cos \alpha \\ \quad = \varphi \left[ \left( \varphi \frac{r}{V_{lb}} + \cos \beta - \varphi \sin \beta \right) \sin \alpha - \varphi \frac{r}{V_{lb}} \right] \\ \quad \quad \sin \alpha = 1 - \frac{BS_{HR}}{V_{lb}} \\ \quad \quad \sin \beta = \frac{r}{V_{lb}} (1 - \sin \alpha) \end{array} \right. \quad (19)$$

where  $\eta$  is the argument to simplify the equation, which can be represented as  $\eta = \left[ 1 - \varphi \frac{r}{V_{lb}} - (1 + \varphi^2) \frac{l}{V_{lb}} \right] / \varphi$ ,  $\beta$  is the angle between the connecting line of the center points of the front and rear wheels and the horizontal plane, and  $\alpha$  is the angle between the force applied to the wheel and the horizontal plane.

Referring to [9], there is a certain relationship between the width of the ditch  $BD_w$  that the vehicle can cross and the passable height of the step  $BS_H$  (see Equation (20)).

$$\frac{BD_w}{2r} = 2\sqrt{\frac{BS_H}{2r} - \left(\frac{BS_H}{2r}\right)^2} \quad (20)$$

The traversability of fences is primarily determined by whether the minimum clearance height of the fence meets the vehicle's passing requirements. While specialized vehicles, such as military vehicles, may be able to drive against weak fences, it is not recommended for ordinary vehicles due to safety concerns.

### 3.3. Traversability Cost Analysis

A wheeled vehicle traversability cost model is developed based on simulation test data from various terrains. Subsequently, the traversability cost for each region is assessed using the obtained traversability boundary map and the established traversability cost model, resulting in the creation of a traversability cost map.

In this paper, the traversability cost model takes into account the height, slope, friction, roughness, and obstacles. The cost model described in the literature [27,28] integrated parameters such as the slope, roughness, and steps, assuming a consistently linear relationship between the traversability cost and parameter values. In reality, the relationship between the traversability cost and parameter value is not constant. When the parameter value is small, its impact on traversability cost is minimal, resulting in a smaller proportion of the relationship; conversely, when the parameter value is large, its impact on traversability cost is significant, leading to a larger proportion of the relationship. Consequently, the traversability cost function can be defined based on how parameter values influence traversability costs within different ranges through experiments or simulation tests. The influence of these parameters on the traversability cost can be evaluated through the limitations imposed on the vehicle speed, with a higher speed limit resulting in a higher traversability cost [29]. Furthermore, these parameters significantly impact the vehicle's load-bearing capacity during traversal, subsequently influencing the traversability cost. Therefore, the impact of various parameters on both the vehicle speed and load capacity is studied in this paper through simulation tests. Subsequently, the traversability cost functions are defined based on the comprehensive analysis of the simulation data.

#### 3.3.1. Terrain Height Cost Definition

The terrain height cost function is generally designed to take into account the change in height when calculating the distance between two points:

$$T_Z = \sqrt{(x_i - x_n)^2 + (y_i - y_n)^2 + [w_z \cdot (z_i - z_n)]^2} \quad (21)$$

where  $T_Z$  is the terrain height cost,  $(x_i, y_i, z_i)$  and  $(x_n, y_n, z_n)$  are the coordinates for any two points, respectively, and  $w_z$  is the weight of the height.



### 3.3.2. Terrain Slope, Friction and Roughness Cost Definition

Experiments or simulation tests can provide insight into the impact of terrain parameters such as the slope, friction, and roughness on the vehicle speed and load. The Chrono platform [30] is utilized to investigate the influence of different terrain parameters on vehicle speed and load-bearing capacity restrictions within the above traversability boundary conditions. Subsequently, traversability cost functions are established based on the influence rule using segmented linear regression methods.

This paper employs simulation test data to examine the maximum average driving speeds of vehicles under different loads on varying terrain slope, friction, and roughness conditions, as illustrated in Figure 3. The maximum average driving speed of a vehicle refers to the maximum mean speed of a vehicle that is capable of meeting acceleration, braking, steering, and vibration requirements smoothly across various terrains without skidding or rolling. Based on the simulation results and empirical knowledge, the slope cost functions (see Equation (22)), friction cost functions (see Equation (23)), and roughness cost functions (see Equation (24)) are established through segmented linear regression.

$$T_S = \begin{cases} k_{s1} \frac{S}{S_L}, & S \leq S_F \\ T_{S1} + k_{s2} \frac{S}{S_L}, & S_F < S \leq S_S \\ T_{S2} + k_{s3} \frac{S}{S_L}, & S_S < S \leq S_L \end{cases} \quad (22)$$

$$T_\varphi = \begin{cases} k_{f1} \frac{\varphi}{\varphi_F}, & \varphi \geq \varphi_F \\ T_{\varphi1} + k_{f2} \frac{\varphi}{\varphi_F}, & \varphi_S \leq \varphi < \varphi_F \\ T_{\varphi2} + k_{f3} \frac{\varphi}{\varphi_F}, & \varphi_L \leq \varphi < \varphi_S \end{cases} \quad (23)$$

$$T_R = \begin{cases} k_{r1} \frac{R}{R_L}, & R \leq R_F \\ T_{R1} + k_{r2} \frac{R}{R_L}, & R_F < R \leq R_L \end{cases} \quad (24)$$

where  $T_S$ ,  $T_\varphi$ , and  $T_R$  are the slope, friction, and roughness costs;  $S$ ,  $\varphi$ , and  $R$  are the actual slope, friction, and roughness of the terrain, where  $S$  is calculated with the driving direction  $\theta$ ;  $S_F$ ,  $\varphi_F$ , and  $R_F$  are the free thresholds of slope, friction, and roughness at which the vehicle can traverse with lower cost;  $S_S$  and  $\varphi_S$  represent the risky thresholds of slope and friction at which the vehicle can traverse with higher cost;  $S_L$ ,  $\varphi_L$ , and  $R_L$  are the traversability boundary conditions of slope, friction, and roughness that were identified in the previous section;  $k_{si}$ ,  $k_{fi}$ ,  $k_{ri}$ ,  $T_{Si}$ ,  $T_{\varphi i}$ , and  $T_{Ri}$  ( $i = 1, 2, 3$ ) are the parameters of these functions that can be selected according to the simulation tests.

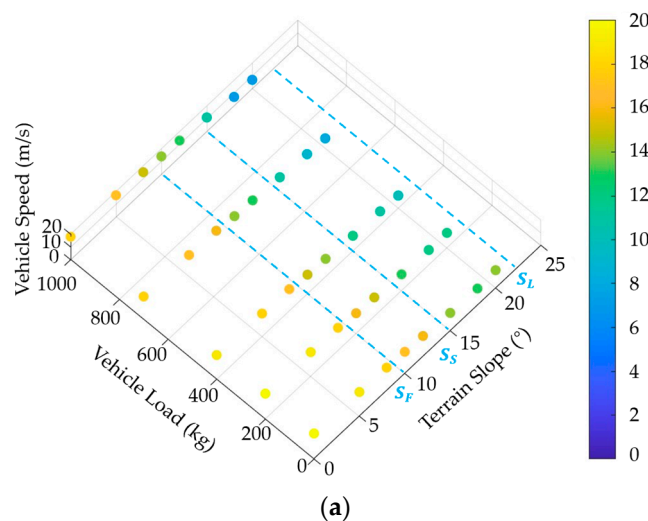
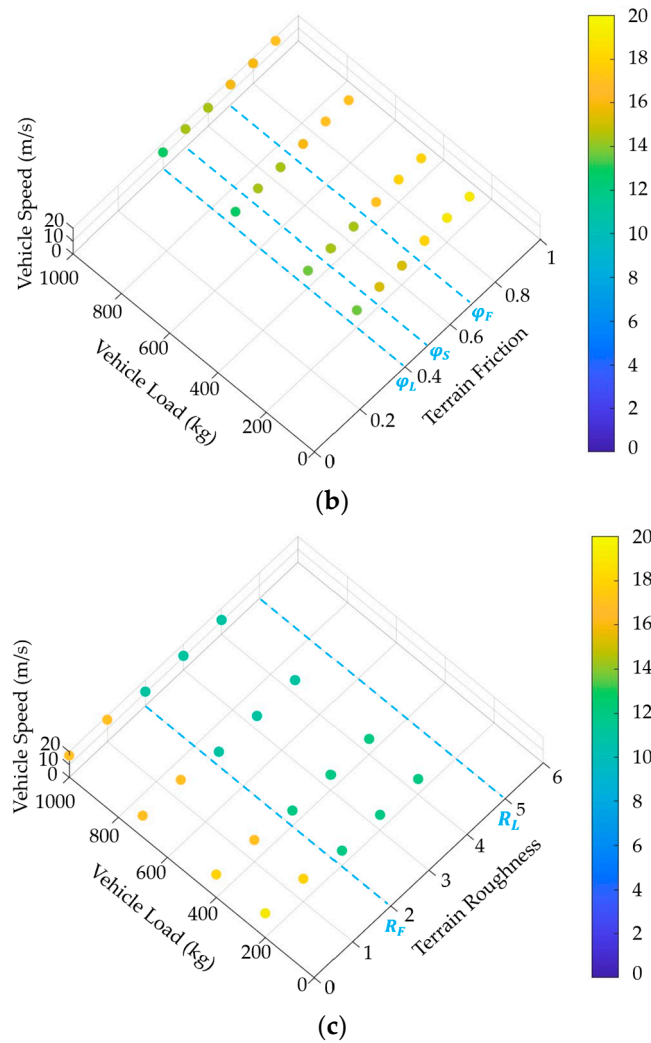


Figure 3. Cont.



**Figure 3.** The relationship among vehicle speed, vehicle load, and terrain parameters: (a) The maximum average driving speed of vehicles under different loads on varying terrain slopes with favorable friction and roughness conditions; (b) The maximum average driving speed of vehicles under different loads on varying friction conditions of flat terrain with favorable roughness conditions; (c) The maximum average driving speed of vehicles under different loads on varying roughness conditions of flat terrain with favorable friction conditions. The x-axis values 1–8 correspond to the roughness categories A–H.

### 3.3.3. Terrain Obstacle Cost Definition

According to the literature [22] and experience, the traversability cost of obstacles can be qualitatively classified based on their types. For example, low grass and trees with free gaps result in a lower speed drop for vehicles, while high grass, trees with safe gaps, speed bumps, low steps, small ditches, and high traversable fences lead to a medium speed drop. Bushes, high steps, large ditches, and low traversable fences are considered limited obstacles that result in a higher speed drop for vehicles. The traversability cost of terrain obstacles  $T_U$  is defined based on the following classification:

$$T_U = \begin{cases} T_{U1}, & I_F = \{Low\ Grass, Trees\ with\ free\ gaps\} \\ T_{U2}, & I_s = \{High\ Grass, Trees\ with\ safe\ gaps, Speed\ bumps, Low\ Steps, \\ & Small\ Ditches, High\ traversable\ fence\} \\ T_{U3}, & I_L = \{Bush, High\ Steps, Large\ Ditches, Low\ traversable\ fence\} \end{cases} \quad (25)$$

where  $T_{U1}$ ,  $T_{U2}$ , and  $T_{U3}$  represent the respective traversability cost of the obstacles corresponding to the classification of  $I_F$ ,  $I_s$ , and  $I_L$ .

### 3.4. Path Planning

In the Hybrid A\* algorithm, the path cost  $f(x)$  comprises both  $g(x)$  and  $h(x)$ .

$$f(x) = g(x) + h(x) \quad (26)$$

where  $g(x)$  is the cost of the path from the starting point to the current point, and  $h(x)$  is the estimated cost of the path from the current point to the end point.

In the Hybrid A\* algorithm, the function  $g(x)$  accounts for the physical distance traveled from the starting point to the current point and considers the wheeled vehicle's maneuvers (such as reversing, advancing, turning, etc.) without taking into account the terrain and vehicle characteristics. Environmental factors such as the slope, step, and other obstacles were considered in designing  $g(x)$  in [12]. In Section 3.3, the impact of individual terrain parameters on the wheeled vehicle traversability cost is separately addressed, while the consideration of different parameters' influence on the wheeled vehicle path cost should be approached contrastively during path planning. The TV-Hybrid A\* algorithm proposed in this paper reconfigures the  $g(x)$  cost function to account for both terrain and vehicle characteristics:

$$g(x) = \sum[(\omega_Z T_{Z_{n_{ave}}} + \omega_R T_{R_{n_{ave}}} + \omega_F T_{F_{n_{ave}}} + \omega_S T_{n_{ave}} + \omega_U T_{U_{n_{ave}}}) \cdot \Delta l_n + g_{maneuver\_n}] \quad (27)$$

where  $\omega_j$  ( $j = Z, R, F, S, U$ ) are the weight of the terrain height, roughness, friction, slope, and obstacles costs, which can be determined by the simulation test data and neutral network method;  $T_{j_{n_{ave}}}$  ( $j = Z, R, F, S, U$ ) are the mean traversability costs of the terrain height, roughness, friction, slope, and obstacles from position point  $n$  to point  $n + 1$ , which can be calculated by Equation (28);  $\Delta l_n$  is the distance between position point  $n$  and point  $n + 1$ ;  $g_{maneuver\_n}$  is the extra penalty costs of vehicle maneuvering from position point  $n$  to point  $n + 1$ .

$$T_{j_{n_{ave}}} = \frac{\sum(T_{j_{nk}} \cdot \Delta l_{nk})}{\Delta l_n} (j = Z, R, F, S, U; k = 1, 2, \dots) \quad (28)$$

where  $k$  denotes the various terrain types that may be traversed from point  $n$  to point  $n + 1$ , and  $T_{j_{nk}}$  and  $\Delta l_{nk}$  represent the respective cost and length of each type from point  $n$  to point  $n + 1$ .

This paper presents a three-layer neural network model established using data on the maximum vehicle speed and maximum load under different terrain parameters obtained from simulation tests. The model aims to contrastively analyze the impact of various parameters on path costs, as illustrated in Figure 4. The neural network model is composed of a single hidden layer, containing precisely 10 neurons. This hidden layer employs the tansig activation function, which introduces nonlinearity and facilitates the network's ability to capture complex patterns in the data. Meanwhile, the output layer utilizes the purelin activation function, ensuring a linear mapping of the hidden layer's output to the final prediction [31]. The influence of terrain parameters on vehicle path costs can be roughly estimated by scrutinizing the weights assigned to the first layer of the neural network, which connects the input layer to the hidden layer. Furthermore, sensitivity analysis facilitates a more nuanced evaluation of how each parameter contributes to the overall vehicle path costs.

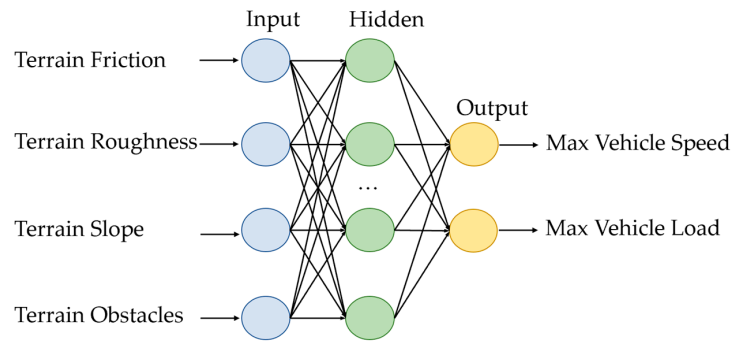


**Figure 4.** A three-layer neural network to analyze the impact of terrain parameters on path costs.

## 4. Results

### 4.1. Simulation Framework

The simulation environment excels at conducting parametric modeling of the terrain with various parameters and targeted validation. Consequently, the traversability analysis and path planning methods on rigid terrains are validated through simulation in this paper. The generated path by the TV-Hybrid A\* planner is compared with that of A\* and Hybrid A\*. The entire simulation framework is illustrated in Figure 5. Solidworks is utilized for creating the initial environment model, while MATLAB processes environmental information, conducts traversability analysis, and conducts path planning, including creating initial environment maps, establishing traversability boundary conditions to generate a traversability boundary map, establishing traversability cost functions to generate a traversability cost map, and implementing the TV-Hybrid A\* algorithm to generate a planning path. Additionally, Chrono [30,32,33] is used for creating vehicle models, simulating vehicle traversability for different terrain parameters based on environmental information, verifying paths generated by TV-Hybrid A\*, and comparing them with paths generated by A\* and Hybrid A\*. Chrono is extensively utilized for vehicles across various terrains, including rigid, deformable, and granular terrains [30,32,33]. It can perform high-fidelity simulations of terrains, wheels, and terrain mechanics.

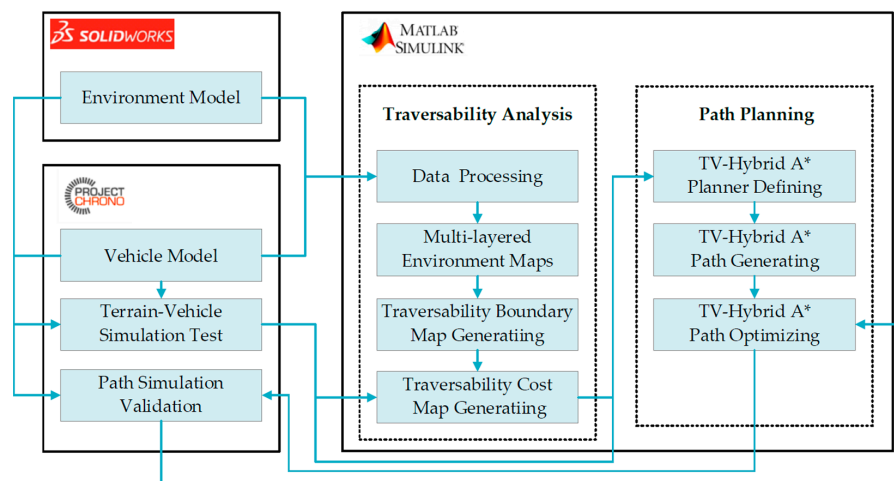


**Figure 5.** The simulation validation framework for traversability analysis and path planning methods on rigid terrains.

### 4.2. Simulation Model

#### 4.2.1. Terrain Model

In this paper, a 200 m × 200 m 3D terrain model is designed and meshed with a cell size of 1 m × 1 m, on which the terrain slope, friction, roughness, and obstacles are randomly configured as depicted in Figure 6.

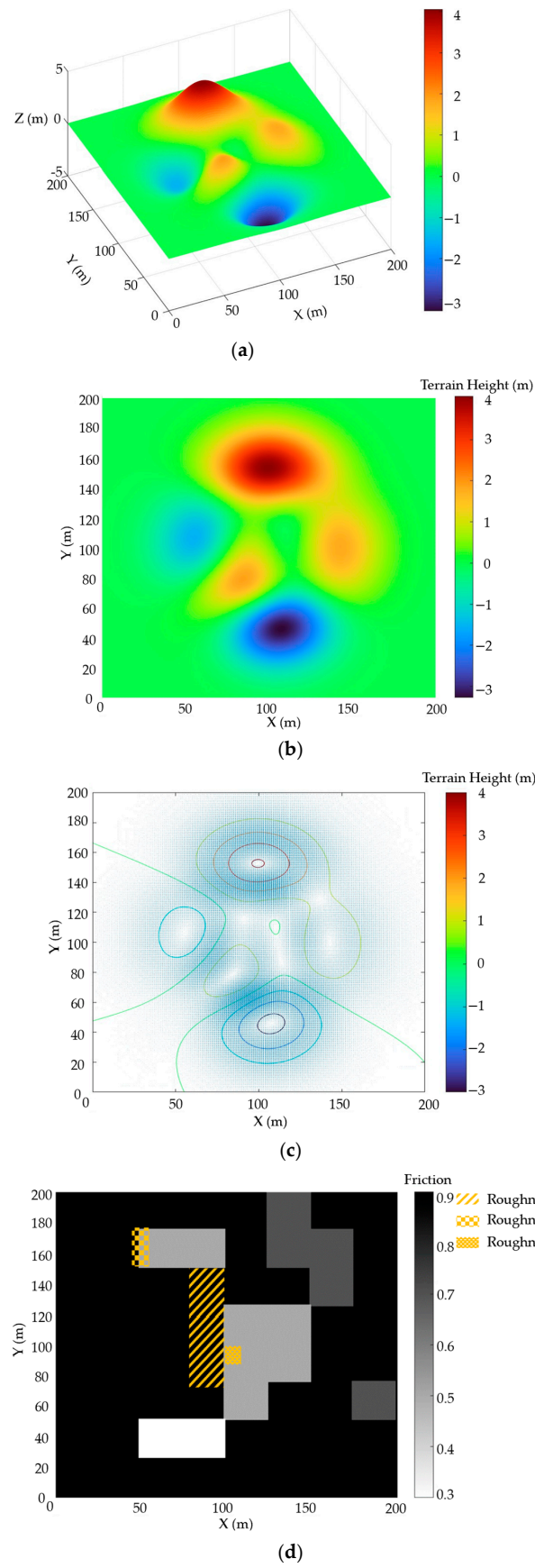
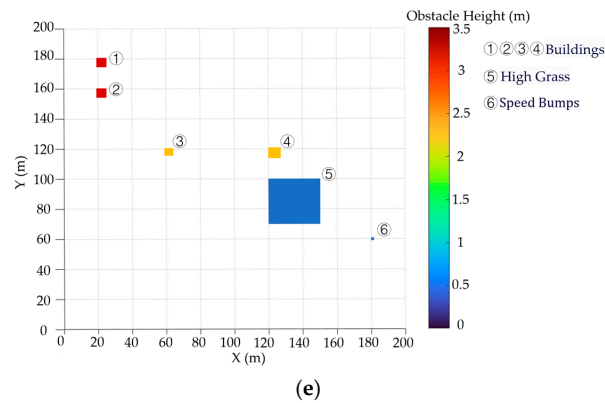


Figure 6. Cont.



**Figure 6.** The initial environmental information for the simulation validation: (a) The terrain DEM model; (b) The terrain height map obtained from the DEM model; (c) The terrain gradient map obtained from the DEM model; (d) The terrain physical distribution information of friction marked in gray with roughness marked with filling; (e) The terrain obstacles with height and type information.

#### 4.2.2. Vehicle Model

A prototype vehicle model is employed as a case study to evaluate its performance in the aforementioned terrain environment, as depicted in Figure 7. This model takes into account the translational motions of the vehicle in the x, y, and z directions; the yaw, pitch, and roll motions; and the rolling, steering, and vertical motions of the wheels. The vehicle model is rear-wheel drive with a mass of 4140 kg, and other specific vehicle parameters are provided in Table 1.

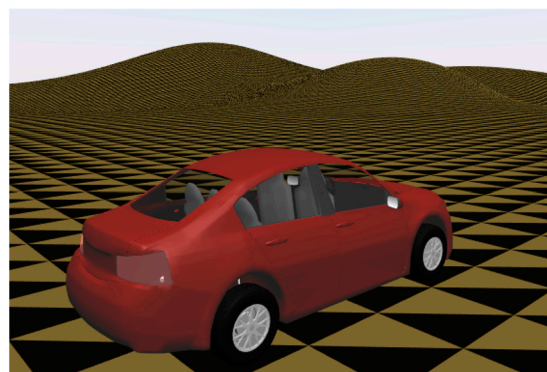


**Figure 7.** The simulation model of the articulated chassis vehicle on the designed terrain.

**Table 1.** The parameters of the vehicle model.

| Parameter                | Value | Units |
|--------------------------|-------|-------|
| Vehicle Length           | 4.84  | m     |
| Vehicle Width            | 2     | m     |
| Minimum Ground Clearance | 0.3   | m     |
| Wheel Radius             | 0.42  | m     |
| Wheelbase                | 4     | m     |
| Maximum Engine Torque    | 300   | N·m   |
| Maximum Engine Power     | 110   | kW    |
| Maximum Braking Torque   | 4000  | N·m   |
| Minimum Turning Radius   | 5     | m     |
| Maximum Steering Angle   | 135   | °     |

### 4.3. Simulation Results

#### 4.3.1. Traversability Boundary and Cost Map

The traversability boundary map is generated based on the designed terrain and vehicle model according to the established boundary conditions, as depicted in Figure 8. The cost map is obtained through traversability cost analysis of the height, slope, friction, roughness, and obstacles within traversable areas, as shown in Figure 9. This includes calculating the slope cost along both the  $x$ - and  $y$ -direction gradients. The costs for other driving directions can be derived from the  $x$  and  $y$  costs.

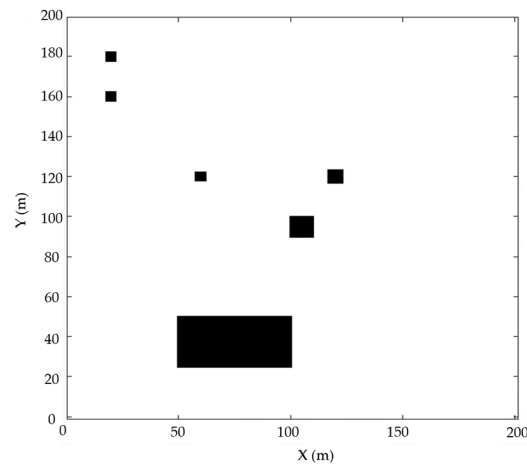


Figure 8. Traversability boundary map with black areas indicating impassable areas.

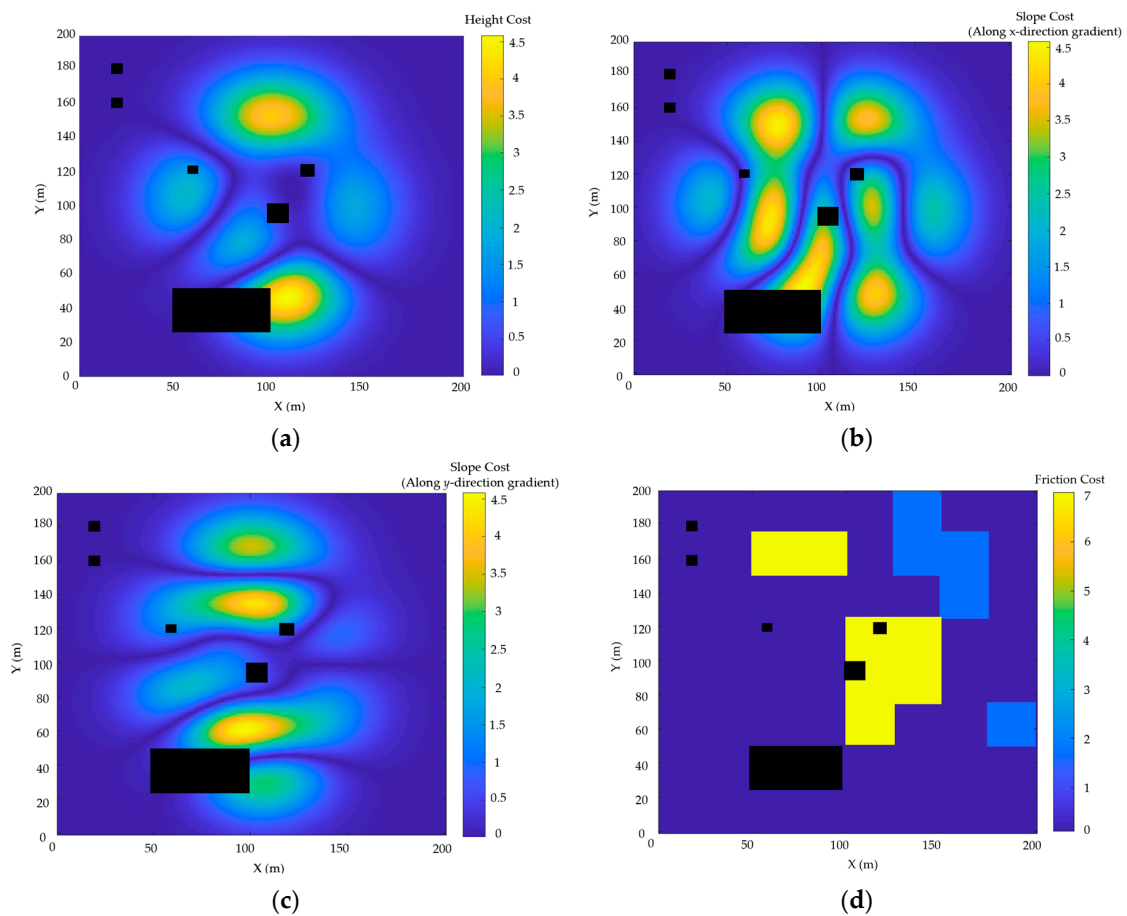
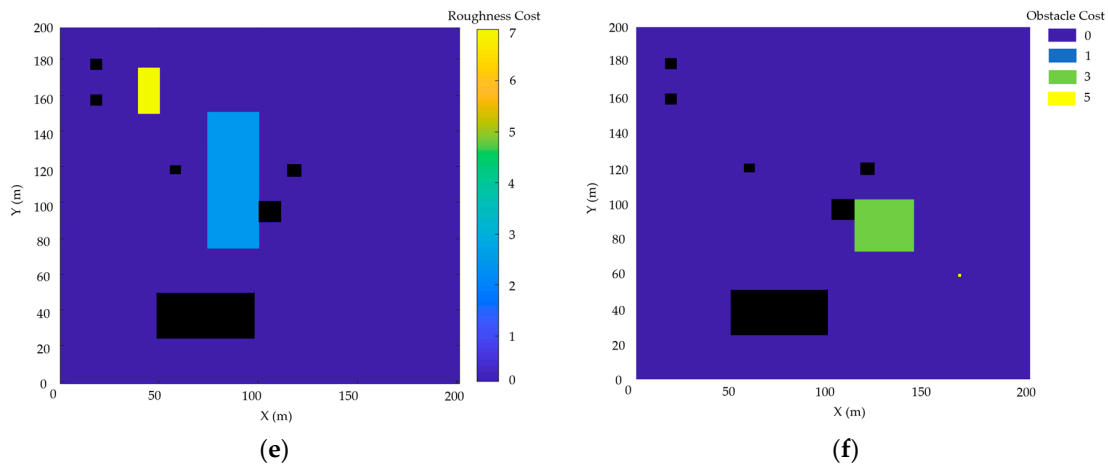


Figure 9. Cont.



**Figure 9.** The traversability cost maps with the impassable areas marked in black: (a) Height cost map; (b) Slope cost map along  $x$ -direction gradient; (c) Slope cost map along  $y$ -direction gradient; (d) Friction cost map; (e) Roughness cost map; (f) Obstacles cost map.

#### 4.3.2. Path Planning

Based on simulation tests and neural network results, it has been determined that the path cost is highly influenced by roughness and obstacles. This finding dictates the selection of weights for terrain parameters in the path cost functions of the TV-Hybrid A\* planner. Then the planned paths are respectively generated by the A\* planner, Hybrid A\* planner, and the TV-Hybrid A\* planner based on the obtained boundary map and cost map.

The path generated by the TV-Hybrid A\* algorithm demonstrates fewer significant deviations but more minor fluctuations compared to that generated by the Hybrid A\* and A\* algorithm from a geometric perspective, as illustrated in Figure 10. Subsequently, three paths are individually simulated in Chrono, and the simulation data of both paths are presented in Table 2. According to the simulation results, in comparison with the A\* planner and Hybrid A\* algorithm, the path generated by TV-Hybrid A\* exhibits a slightly shorter length, reduced travel time and energy consumption, and a marginally higher average vehicle speed. This suggests that the selected path terrain imposes a slightly lower speed limit and traversability cost on the vehicle. Ultimately, regarding computational efficiency, Table 2 clearly showcases the reduced path generation duration achieved. The algorithm introduced in this paper exhibits superior performance over the conventional A\* planner and Hybrid A\* algorithm for this terrain model. This enhanced efficiency stems from the initial delineation of traversable boundaries, effectively pruning unnecessary computations and evaluations in impassable areas. Additionally, the pre-emptive analysis of traversability costs within the static environment during traversability assessment further contributes to time savings during path planning, resulting in a more streamlined and efficient process.

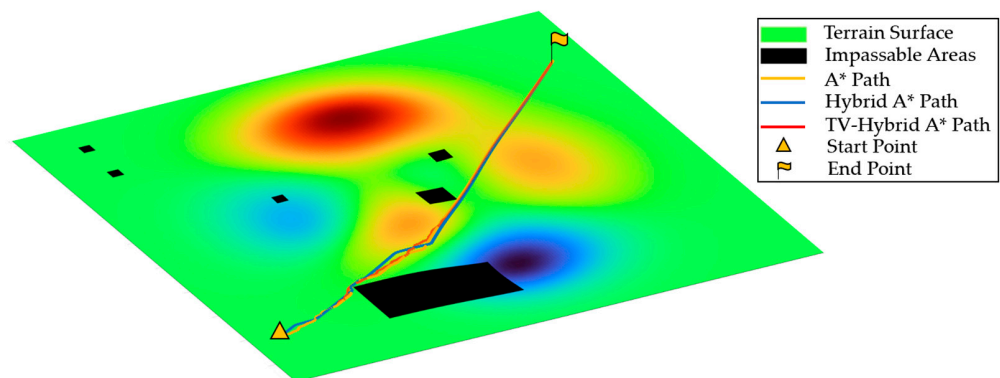


**Figure 10.** The paths generated by the Hybrid A\* and TV-Hybrid A\* planners.



**Table 2.** The comparison data for the two paths.

| Path         | Path Length (m) | Travel Time (s) | Average Speed (m/s) | Energy (J) | Calculation Time (s) |
|--------------|-----------------|-----------------|---------------------|------------|----------------------|
| A*           | 228.4           | 23.4            | 9.76                | 1912       | 0.49                 |
| Hybrid A*    | 227.6           | 23.1            | 9.85                | 1844       | 0.34                 |
| TV-Hybrid A* | 226.8           | 22.8            | 9.94                | 1734       | 0.27                 |

## 5. Conclusions

A traversability analysis and path planning framework for wheeled vehicles on rigid terrains was proposed in this paper. The traversability boundary conditions were first analyzed to obtain the boundary map of the traversable areas, and then the traversability cost analysis and path planning based on this were conducted. This framework avoids redundant analysis and calculation of impassable areas while enhancing the cost-effectiveness of the planned path.

During the traversability boundary analysis, the geometric, physical, and obstacle traversable conditions were established based on theoretical principles and practical experience, taking into account the characteristics of both the terrain and wheeled vehicles. For the geometric boundary, a comprehensive analysis of slope conditions was conducted, considering various driving directions. The limit conditions of friction and roughness were analyzed for the physical boundary, considering vehicle driving stability and comfort. The obstacle boundary conditions, including vegetation, steps, ditches, and fences, were analyzed based on their type, size, and distribution. The traversability costs of the terrain height, slope, friction, roughness, and obstacles were analyzed in this paper. The height cost was defined as the distance cost associated with the height change. The traversability costs of the slope, friction, and roughness were evaluated based on the limitations imposed by terrain parameters on the vehicle speed and load in simulations. Based on the simulation data, the traversability cost functions of the slope, friction, and roughness were then established by the segmented linear regression method. The cost of obstacles was defined by a qualitative classification. In path planning, the path cost function was redefined in this paper with the proposed TV-Hybrid A\* algorithm, which was based on the Hybrid A\* algorithm. This path cost function was based on the simulation data and a three-layer neural network model, with consideration for the characteristics of the terrain and vehicle. The paths planned by A\*, Hybrid A\*, and TV-Hybrid A\* were each validated in the simulation, showing that TV-Hybrid A\* resulted in a shorter path length, less travel time, and less energy consumption due to consideration of the terrain and vehicle characteristics.

The traversability analysis and path planning methodologies presented in this paper hold the potential to substantially optimize path costs, yet there remain avenues for improvement to address inherent limitations. Firstly, while enhancing the computational efficiency of path planning, the approach faces a significant challenge in scaling to complex, real-world environments, where the computational burden of traversability analysis becomes substantial. Future work should focus on refining and optimizing these algorithms through rigorous testing in real-world environments, ensuring their performance and adaptability in practical applications. Secondly, the current definitions of traversability boundary conditions are narrowly focused on rigid terrains, which limits their applicability to the broader range of dynamic and deformable terrains encountered in nature. To expand the versatility of these methods, it is imperative to incorporate terrain mechanics principles, allowing for a more nuanced assessment of the terrain properties that influence traversability.

In the future, this study will be expanded to include fleet applications and integrated with technologies such as the Internet of Things and cloud computing for better three-dimensional transportation systems in mining, rescue, construction, and the military.

**Author Contributions:** Conceptualization, N.W., X.L., J.W. and D.X.; methodology, N.W., J.W. and D.X.; software, N.W.; validation, N.W. and X.L.; formal analysis, Z.S. and J.F.; investigation, N.W.; writing—original draft preparation, N.W., X.L., Z.S., J.F., J.W. and D.X.; writing—review and editing, N.W., X.L., J.W. and D.X.; visualization, N.W., X.L., Z.S. and J.F.; supervision, J.W. and D.X.; project administration, J.W. and D.X.; funding acquisition, J.W. and D.X. All authors have read and agreed to the published version of the manuscript.

**Funding:** This research was funded by the National Natural Science Foundation of China (Grant number 52272434), the Scientific research project of the Education Department of Jilin Province (Grant number JJKH20240848KJ), and the Natural Science Foundation of Jilin Province (Grant number YDZJ202401593ZYTS).

**Data Availability Statement:** Data will be made available on request.

**Conflicts of Interest:** The authors declare no conflicts of interest.

## References

- Bai, Y.; Zhang, B.; Xu, N.; Zhou, J.; Shi, J.; Diao, Z. Vision-Based Navigation and Guidance for Agricultural Autonomous Vehicles and Robots: A Review. *Comput. Electron. Agric.* **2023**, *205*, 107584. [[CrossRef](#)]
- He, X.; Wu, J.; Huang, Z.; Hu, Z.; Wang, J.; Sangiovanni-Vincentelli, A.; Lv, C. Fear-Neuro-Inspired Reinforcement Learning for Safe Autonomous Driving. *IEEE Trans. Pattern Anal. Mach. Intell.* **2023**, *46*, 267–279. [[CrossRef](#)] [[PubMed](#)]
- He, X.; Huang, W.; Lv, C. Toward Trustworthy Decision Making for Autonomous Vehicles: A Robust Reinforcement Learning Approach with Safety Guarantees. *Engineering* **2023**, *33*, 77–89. [[CrossRef](#)]
- Wallin, E.; Wiberg, V.; Vesterlund, F.; Holmgren, J.; Persson, H.J.; Servin, M. Learning Multiobjective Rough Terrain Traversability. *J. Terramech.* **2022**, *102*, 17–26. [[CrossRef](#)]
- Wang, N.; Li, X.; Zhang, K.; Wang, J.; Xie, D. A Survey on Path Planning for Autonomous Ground Vehicles in Unstructured Environments. *Machines* **2024**, *12*, 31. [[CrossRef](#)]
- Islam, F.; Nabi, M.M.; Ball, J.E. Off-Road Detection Analysis for Autonomous Ground Vehicles: A Review. *Sensors* **2022**, *22*, 8463. [[CrossRef](#)]
- Guastella, D.C.; Muscato, G. Learning-Based Methods of Perception and Navigation for Ground Vehicles in Unstructured Environments: A Review. *Sensors* **2021**, *21*, 73. [[CrossRef](#)]
- Xue, H.; Fu, H.; Xiao, L.; Fan, Y.; Zhao, D.; Dai, B. Traversability Analysis for Autonomous Driving in Complex Environment: A LiDAR-Based Terrain Modeling Approach. *J. Field Robot.* **2023**, *40*, 1779–1803. [[CrossRef](#)]
- Kejian, Z. *Vehicle-Terrainmechanics*; National Defense Industry Press: Beijing, China, 2002.
- Zhu, Z.; Li, N.; Sun, R.; Zhao, H.; Xu, D. Off-Road Autonomous Vehicles Traversability Analysis and Trajectory Planning Based on Deep Inverse Reinforcement Learning. In Proceedings of the 2020 IEEE Intelligent Vehicles Symposium (IV), Las Vegas, NV, USA, 19 October 2020; pp. 971–977.
- He, X.; Huang, W.; Lv, C. Trustworthy Autonomous Driving via Defense-Aware Robust Reinforcement Learning against Worst-Case Observational Perturbations. *Transp. Res. Part C Emerg. Technol.* **2024**, *163*, 104632. [[CrossRef](#)]
- Zhang, Y.; Wang, W.; Bonatti, R.; Maturana, D.; Scherer, S. Integrating Kinematics and Environment Context into Deep Inverse Reinforcement Learning for Predicting Off-Road Vehicle Trajectories. *arXiv* **2018**, arXiv:1810.07225. [[CrossRef](#)]
- Liu, M.; Xie, H.; Pan, W.; Ding, S.; Li, G. Prediction of Cutting Force via Machine Learning: State of the Art, Challenges and Potentials. *J. Intell. Manuf.* **2023**. [[CrossRef](#)]
- Quann, M.; Ojeda, L.; Smith, W.; Rizzo, D.; Castanier, M.; Barton, K. Power Prediction for Heterogeneous Ground Robots through Spatial Mapping and Sharing of Terrain Data. *IEEE Robot. Autom. Lett.* **2020**, *5*, 1579–1586. [[CrossRef](#)]
- Gonzalez, R.; Iagnemma, K. DeepTerramechanics: Terrain Classification and Slip Estimation for Ground Robots via Deep Learning. *arXiv* **2018**, arXiv:1806.07379. [[CrossRef](#)]
- Bae, J.; Seo, J.; Kim, T.; Jeon, H.G.; Kwak, K.; Shim, I. Self-Supervised 3D Traversability Estimation with Proxy Bank Guidance. *IEEE Access* **2023**, *11*, 51490–51501. [[CrossRef](#)]
- Chavez-Garcia, R.O.; Guzzi, J.; Gambardella, L.M.; Giusti, A. Learning Ground Traversability from Simulations. *IEEE Robot. Autom. Lett.* **2018**, *3*, 1695–1702. [[CrossRef](#)]
- Qin, H.; Shao, S.; Wang, T.; Yu, X.; Jiang, Y.; Cao, Z. Review of Autonomous Path Planning Algorithms for Mobile Robots. *Drones* **2023**, *7*, 211. [[CrossRef](#)]
- Li, Z.; Zhao, P.; Jiang, C.; Huang, W.; Liang, H. A Learning-Based Model Predictive Trajectory Planning Controller for Automated Driving in Unstructured Dynamic Environments. *IEEE Trans. Veh. Technol.* **2022**, *71*, 5944–5959. [[CrossRef](#)]
- Abdulsahab, J.A.; Kadhim, D.J. Classical and Heuristic Approaches for Mobile Robot Path Planning: A Survey. *Robotics* **2023**, *12*, 93. [[CrossRef](#)]
- Oliveira, F.G.; Neto, A.A.; Howard, D.; Borges, P.; Campos, M.F.M.; Macharet, D.G. Three-Dimensional Mapping with Augmented Navigation Cost through Deep Learning. *J. Intell. Robot. Syst.* **2021**, *101*, 50. [[CrossRef](#)]

22. Guan, T.; He, Z.; Song, R.; Zhang, L. TNES: Terrain Traversability Mapping, Navigation and Excavation System for Autonomous Excavators on Worksite. *Auton. Robot.* **2023**, *47*, 695–714. [[CrossRef](#)]
23. Chi, Z.; Yu, Z.; Wei, Q.; He, Q.; Li, G.; Ding, S. High-Efficiency Navigation of Nonholonomic Mobile Robots Based on Improved Hybrid A\* Algorithm. *Appl. Sci.* **2023**, *13*, 6141. [[CrossRef](#)]
24. Min, H.; Xiong, X.; Wang, P.; Yu, Y. Autonomous Driving Path Planning Algorithm Based on Improved A\* Algorithm in Unstructured Environment. *Proc. Inst. Mech. Eng. Part D J. Automob. Eng.* **2021**, *235*, 513–526. [[CrossRef](#)]
25. Goulet, N.; Ayalew, B. Energy-Optimal Ground Vehicle Trajectory Planning on Deformable Terrains. *IFAC-PapersOnLine* **2022**, *55*, 196–201. [[CrossRef](#)]
26. ISO 8608:2016. Available online: [https://www.intertekinform.com/en-us/standards/iso-8608-2016-586293\\_saig\\_iso\\_iso\\_134277\\_2/](https://www.intertekinform.com/en-us/standards/iso-8608-2016-586293_saig_iso_iso_134277_2/) (accessed on 25 July 2024).
27. Leung, T.H.Y.; Ignatyev, D.; Zolotas, A. Hybrid Terrain Traversability Analysis in Off-Road Environments. In Proceedings of the 2022 8th International Conference on Automation, Robotics and Applications, ICARA 2022, Prague, Czech Republic, 18–20 February 2022; Institute of Electrical and Electronics Engineers Inc.: Piscataway, NJ, USA, 2022; pp. 50–56.
28. Lee, H.; Kwon, J.; Kwon, C. Learning-Based Uncertainty-Aware Navigation in 3D Off-Road Terrains. In Proceedings of the 2023 IEEE International Conference on Robotics and Automation (ICRA), London, UK, 29 May 2023; pp. 10061–10068.
29. Heštera, H.; Pahernik, M. Physical-Geographic Factors of Terrain Trafficability of Military Vehicles According to Western World Methodologies. *Hrvat. Geogr. Glas.* **2018**, *80*, 5–31. [[CrossRef](#)]
30. Serban, R.; Taylor, M.; Negrut, D.; Tasora, A. Chrono::Vehicle: Template-Based Ground Vehicle Modelling and Simulation. *Int. J. Veh. Perform.* **2019**, *5*, 18–39. [[CrossRef](#)]
31. Dallas, J.; Cole, M.P.; Jayakumar, P.; Ersal, T. Neural Network Based Terramechanics Modeling and Estimation for Deformable Terrains. *arXiv* **2020**, arXiv:2003.02635. [[CrossRef](#)]
32. Recuero, A.; Serban, R.; Peterson, B.; Sugiyama, H.; Jayakumar, P.; Negrut, D. A High-Fidelity Approach for Vehicle Mobility Simulation: Nonlinear Finite Element Tires Operating on Granular Material. *J. Terramech.* **2017**, *72*, 39–54. [[CrossRef](#)]
33. Benatti, S.; Young, A.; Elmquist, A.; Taves, J.; Tasora, A.; Serban, R.; Negrut, D. End-to-End Learning for off-Road Terrain Navigation Using the Chrono Open-Source Simulation Platform. *Multibody Syst. Dyn.* **2022**, *54*, 399–414. [[CrossRef](#)]

**Disclaimer/Publisher’s Note:** The statements, opinions and data contained in all publications are solely those of the individual author(s) and contributor(s) and not of MDPI and/or the editor(s). MDPI and/or the editor(s) disclaim responsibility for any injury to people or property resulting from any ideas, methods, instructions or products referred to in the content.